Identification of Key Regions Mediating Human Melatonin Type 1 Receptor Functional Selectivity Revealed by Natural Variants

Alan Hegron, Eunna Huh, Xavier Deupi, Badr Sokrat, Wenwen Gao, Christian Le Gouill, Mickaël Canouil, Mathilde Boissel, Guillaume Charpentier, Ronan Roussel, Beverley Balkau, Philippe Froguel, Bianca Plouffe, Amélie Bonnefond, Olivier Lichtarge, Ralf Jockers,* and Michel Bouvier*

ACCESS | Metrics & More | Article Recommendations | Supporting Information

ABSTRACT: Melatonin is a hormone mainly produced by the pineal gland and MT_1 is one of the two G protein-coupled receptors (GPCRs) mediating its action. Despite an increasing number of available GPCR crystal structures, the molecular mechanism of activation of a large number of receptors, including MT_1, remains poorly understood. The purpose of this study is to elucidate the structural elements involved in the process of MT_1's activation using naturally occurring variants affecting its function. Thirty-six nonsynonymous variants, including 34 rare ones, were identified in *MTNR1A* (encoding MT_1) from a cohort of 8687 individuals and their signaling profiles were characterized using Bioluminescence Resonance Energy Transfer-based sensors probing 11 different signaling pathways. Computational analysis of the experimental data allowed us to group the variants in clusters according to their signaling profiles and to analyze the position of each variant in the context of the three-dimensional structure of MT_1 to link functional selectivity to structure. MT_1 variant signaling profiles revealed three clusters characterized by (1) wild-type-like variants, (2) variants with selective defect of β-arrestin-2 recruitment, and (3) severely defective variants on all pathways. Our structural analysis allows us to identify important regions for β-arrestin-2 recruitment as well as for Gα12 and Gα15 activation. In addition to identifying MT_1 domains differentially controlling the activation of the various signaling effectors, this study illustrates how natural variants can be used as tools to study the molecular mechanisms of receptor activation.

KEYWORDS: Melatonin, Receptor, GPCR variants, Functional selectivity, Mechanisms of activation
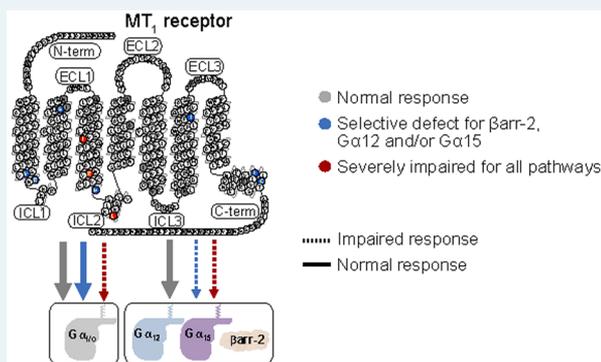
Next-generation sequencing (NGS) is rapidly increasing our understanding of disease causes and susceptibilities in humans as well as of the adaptation and evolution of organisms. Human DNA contains 10,000 to 11,000 non-synonymous genetic variants on average,[1] although only few of them are expected to lead to disease, while the rest are considered neutral. Information on such variants in databases has been often limited to basic annotations like "neutral" or "deleterious". Deleteriousness can be approximated with available information on sequence conservation and molecular functionality, but such data are rarely combined. Furthermore, even a strong association between a mutation and a clinical trait does not provide specific information on the corresponding changes in protein function and/or structure.[2,3] Since just a single genetic variant can change the local structure of a protein or its interactions with other proteins, it can actually have various functional effects.[4] Thus, genetic variants could be instrumental in deciphering molecular determinants and pathways.

Many proteins display several functions by interacting with different protein partners; however, most protein-interaction maps ignore structural details and the mechanisms of protein−protein interaction. This is the case for many G protein-coupled receptors (GPCRs), which can interact with different G proteins, GPCR-regulated kinases (GRKs), and β-arrestins, triggering different signaling pathways. The molecular determinants controlling these different functions are still generally not well understood. It is now known that different ligands can preferentially activate specific GPCR signaling pathways leading to distinct physiological effects. Variants at specific positions in the receptor structure can also modify the
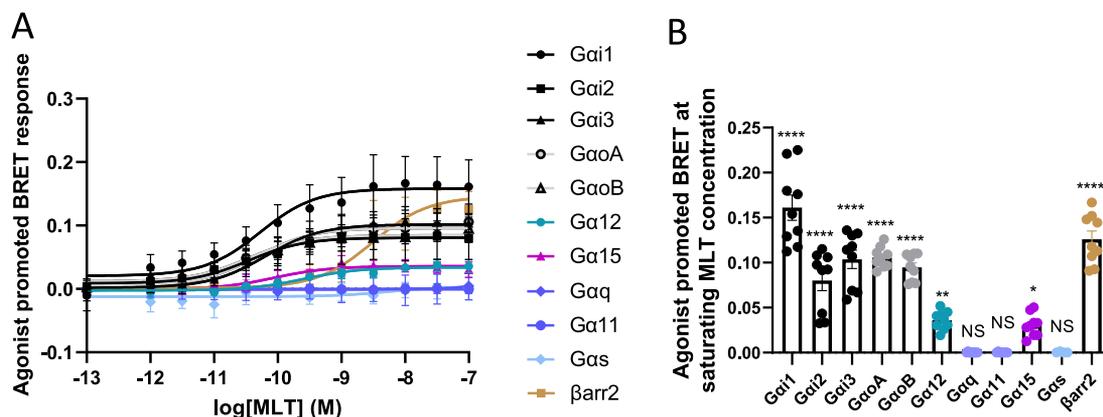
Figure 1. MT$_1$-WT activates Gαi/o, Gα12, Gα15, and recruits βarrestin-2. (A) MLT concentration curves for MT$_1$-WT. Data were plotted using nonlinear regression curves with a fixed Hill slope equal to 1. (B) MT$_1$ response for Gαi1, Gαi2, Gαi3, GαoA, GαoB, Gα12, Gαq, Gα11, Gα15, and Gαs activation and βarrestin-2 recruitment at saturated MLT concentration (100 nM) of the corresponding curves in A. Statistical analysis was performed using one-way ANOVA followed by a Dunnett's posthoc test. Data represents the mean $\pm$ SEM of 5 to 9 experiments. Data were fitted in GraphPad Prism 9. * $p \leq 0.05$, ** $p \leq 0.01$, **** $p \leq 0.0001$. βarr2: βarrestin-2.

activation mechanism and thus the signaling profile of a receptor[5] by inhibiting one or several pathways or, conversely, by promoting others. This concept can be referred to as genetically defined functional selectivity or biased signaling.[6]

We took advantage of the abundance of genetic variants in *MTNR1A* (encoding the melatonin receptor 1 [MT$_1$]) to explore the link between structure and functional selectivity. Melatonin (MLT) is mainly released by the pineal gland in circadian and seasonal manners.[7] The MT$_1$ is one out of two melatonin receptors involved in the physiological action of this neuro-hormone.[8] MT$_1$ expression has been reported in several tissues and organs[9] including the retina,[10,11] brain,[12] pancreas, and immune system.[13,14] MT$_1$ is involved in various physiological functions including circadian entrainment,[15] sleep,[16] dopamine level regulation,[17] and glycemic homeostasis.[18]

In the present study, we identified 36 *MTNR1A* variants and investigated their capacity to activate seven G protein subtypes and to recruit βarrestin-2. We found that these variants can be clustered in three distinct functional groups providing insights into specific structural features of the MT$_1$ underlying functional selectivity.

■ RESULTS

Signaling Profile of Wild-Type MT$_1$. To obtain a comprehensive profiling of the signaling repertoire of MT$_1$, we used bioluminescence resonance energy transfer (BRET)-based biosensors to assess G protein activation measuring Gα protein dissociation from the G$\beta\gamma$ complex[19] (Figure S1A). We measured βarrestin-2 recruitment to the activated receptor measuring its proximity with the plasma membrane using enhanced bystander BRET (ebBRET)[20] (Figure S1B). Melatonin stimulation in cells expressing the wild-type (WT) human MT$_1$ leads to the activation of Gαi1, Gαi2, Gαi3, GαoA, GαoB, Gα12, and Gα15 (Figure 1). This is consistent with previous findings suggesting a predominant coupling to Gαi for this receptor. Gα15, an atypical member of the Gαq/11 family, has been shown to couple in a promiscuous manner to many distinct GPCRs.[21] Because the human embryonic kidney 293 (HEK293) cells used do not express Gα15, its potential activation by MT$_1$ was assessed by probing the downstream activation of protein kinase C (PKC) using a

BRET-based PKC activity sensor[22] (Figure S1C) upon Gα15 expression. The data show that no MLT-promoted PKC activation could be detected in the absence of Gα15, but the addition of Gα15 resulted in a robust PKC activation illustrating the ability of MT$_1$ to functionally engage this protein (Figure 1).

Identification of MT$_1$ Variants and Cell Surface Expression. To identify natural variants, we sequenced the two exons of the *MTNR1A* gene in 8687 unrelated European individuals. We accurately identified 36 genetic variants, including 34 rare variants with a minor allele frequency (MAF) of <1% (Table S1). The two frequent variants are nonsynonymous variants. Among the 34 rare variants, we found 2 nonsense variants introducing STOP codons (p.W93*, p.Y170*), one variant on a donor splice site (c.184 + 1G > T), one frameshift variant (c.999_1014del/p.W333*), one loss of STOP codon variant (c.1053A > T/p.*351Yext* 18 (YKST-TFRVRWTRCARPRS)) and 29 nonsynonymous variants (Table S1). As we previously found that rare deleterious variants in *MTNR1B* (encoding the MT$_2$ receptor) were significantly associated with increased risk of type 2 diabetes,[23] we assessed the association between the coding variants of *MTNR1A* and the risk of type 2 diabetes or obesity. Neither the frequent *MTNR1A* variants (i.e., p.G166E-rs28383653 and p.A266 V-rs28383652) nor the 34 rare *MTNR1A* variants were associated with the risk of type 2 diabetes or obesity in both children and adults (Table S2).

Then, we determined the functional properties of all 32 nonsynonymous MT$_1$ variants in comparison to the MT$_1$-WT in terms of cell surface expression, G protein activation, βarrestin-2 recruitment, and binding of the radioligand 2(^{125}I)-iodomelatonin (^{125}I-MLT).

Cell surface expression of MT$_1$ variants was assessed by enzyme-linked immunosorbent assay (ELISA), detecting the Flag tag located at the extracellular N-terminus of the receptor. Figure S2 shows that similar expression levels were observed for all variants compared to MT$_1$-WT, indicating that the results of the functional assays for the different MT$_1$ variants would not be severely affected by differences in the number of receptors at the cell surface.

Signaling Profiles of MT$_1$ Variants. Melatonin concentration−response curves were generated for each MT$_1$ variant

Table 1. Comparison of Efficacies and Potencies of the Different MT$_1$ Receptors to Activate Gα Proteins and Recruit βarrestin-2[a]

				Emax									EC50				
		Gi1	Gi2	Gi3	GoA	GoB	G12	G15	Barr2	Gi1	Gi2	Gi3	GoA	GoB	G12	G15	Barr2
	WT-MT1	100	100	100	100	100	100	100	100	-10.54	-10.75	-10.4	-10.65	-10.68	-9.84	-9.14	-9
	G18R	104.9	108.3	106.1	121.9	132.4	89.46	83.5	55.8	-10.47	-10.72	-10.45	-10.75	-10.84	-9.73	-9.2	-8.86
	I88V	92.9	108.7	95.67	106.8	116.7	58.97	98.43	30.39	-10.34	-10.55	-10.31	-10.43	-10.43	-9.53	-9.15	-9.18
	N91Y	92.7	103.6	94.15	89.74	94.97	82.38	97.41	78.17	-10.4	-10.87	-10.18	-10.49	-10.5	-9.84	-9.48	-9
	G96D	106.1	91.39	91.5	95.62	126.5	94.22	75.22	71.62	-10.48	-10.58	-10.46	-10.54	-10.64	-9.81	-8.7	-8.57
	A157V	103.9	101.5	94.42	99.66	108.5	93.69	126.5	106.2	-10.4	-10.69	-10.23	-10.5	-10.76	-9.61	-9.52	-8.98
	G166E	116.9	95.86	95.91	124.9	128.7	83.89	60.05	37.96	-10.53	-10.58	-10.3	-10.36	-10.44	-9.76	-8.82	-8.71
	A180T	97.3	95.66	98.31	82.55	72.56	99.08	90.96	112.6	-10.45	-10.67	-10.32	-10.88	-10.6	-10.19	-8.55	-9.17
	I212T	106.2	91.02	93.22	113.7	116.3	87.93	88.05	65.79	-10.38	-10.64	-10.39	-10.6	-10.46	-9.79	-9.15	-8.74
	V221M	126.8	117.8	110.3	95.85	136.7	84.5	136.2	110.9	-10.28	-10.41	-10.27	-10.46	-10.63	-10.04	-8.71	-8.94
	K228R	108.7	105.7	125.2	124.4	133.5	102.7	134.2	143.5	-10.5	-10.71	-10.44	-10.76	-10.75	-10.07	-8.58	-8.72
Cluster 1	A266T	95	95.82	104.6	102.7	101.5	94.77	97.98	96.25	-10.7	-10.76	-10.45	-10.87	-10.85	-10.24	-9.37	-9.07
	A266V	103.5	85.24	95.83	115.3	106.8	94.74	109.6	105.9	-10.69	-10.65	-10.52	-10.72	-10.85	-9.76	-8.77	-8.83
	S267G	103.7	92.13	84.38	108.1	107.3	98.97	93.02	85.42	-10.69	-10.79	-10.33	-10.72	-10.97	-9.89	-8.82	-8.75
	R307S	109.4	89.15	103.1	111.5	132.8	82.27	80.99	44.72	-10.58	-10.6	-10.64	-10.63	-10.65	-9.84	-8.62	-8.72
	V321M	85.6	106	96.09	102	112.6	82.19	112.4	99.99	-10.45	-10.67	-10.2	-10.79	-10.91	-9.72	-9.59	-9.1
	D326N	90	90.44	101.1	102.5	97.87	98.68	101.9	112.5	-10.61	-10.67	-10.19	-10.71	-10.59	-9.92	-9.37	-9.17
	V331F	105.9	105.8	105.3	104.6	110.9	95.75	118.6	76.52	-10.51	-10.76	-10.45	-10.6	-10.73	-9.94	-9.44	-9.11
	K334N	95.7	81.25	103	115	104.2	91.81	109	93.33	-10.6	-10.56	-10.44	-10.52	-10.69	-9.65	-8.79	-8.87
	T340I	108.5	100.3	92.25	110.6	94.81	80.05	102.1	87.13	-10.68	-10.73	-10.58	-10.68	-10.6	-9.77	-9.417	-9.06
	N342S	100.9	86.42	100.8	100.9	112.4	89.22	93.31	95.11	-10.4	-10.66	-10.19	-10.48	-10.61	-9.77	-8.66	-8.68
	V345I	88.5	88.46	95.68	109.3	112.4	93.51	93.19	90.83	-10.53	-10.77	-10.39	-10.47	-10.85	-9.7	-8.72	-8.74
	V52A	64	49.33	39.25	93.59	88.61	15.86	NR	NR	-10.07	-9.81	-9.98	-10.59	-10.18	-7.95	NR	NR
	R54W	91.8	98.79	84.44	98.04	96.33	39.75	54.33	NR	-10.49	-10.48	-10.16	-10.77	-10.45	-10.08	-9.09	NR
	S87L	104.9	108.7	77.33	131.2	147.3	48.06	NR	NR	-10.25	-10.2	-10.22	-10.21	-10.22	-9.06	NR	NR
Cluster 2	H131R	97.6	111.6	102.5	108.2	124.4	45.54	17.84	NR	-10.29	-10.47	-10.09	-10.47	-10.52	-9.47	-8.5	NR
	I257F	77.2	124.3	85.21	105.9	130.1	47.84	79.14	NR	-9.482	-9.998	-9.57	-9.58	-9.83	-9.5	-9.25	NR
	I309T	104.1	126.5	97.78	118.6	143.3	52.89	58.42	NR	-10.09	-10.3	-9.99	-9.92	-10.42	-9.41	-9.14	NR
	C314R	84.2	75.89	76.46	113.8	125.3	57.12	33.11	NR	-10.56	-10.49	-10.2	-10.63	-10.64	-9.78	-8.75	NR
	I112N	65.8	83.08	89.65	71.23	87.96	75.89	60.19	43.35	-8.555	-8.71	-8.49	-8.34	-8.63	-7.66	-8	-7.27
Cluster 3	R125C	NR	53.06	NR	NR	55.41	NR	NR	NR	NR	-7.798	NR	NR	-10.44	NR	NR	NR
	L138P	111.7	109.1	78.62	109.2	140	56.13	26.54	NR	-8.948	-9.015	-9.23	-8.82	-9.12	-8.26	-7.89	NR
	P80L	NR	NR	NR	NR	NR	NR	NR	NR	NR	NR	NR	NR	NR	NR	NR	NR

Emax scale: 200 / 100 / 0. EC50 scale: + 1 Log / WT EC50 / – 1 Log.

[a]Functional profiling of Gα protein activations and βarrestin-2 recruitment by MT$_1$-WT and MT$_1$ variants. Data represents the mean ± SEM of 3-16 independent experiments with repeats in quadruplicate. NR (No response) denotes that the experimental parameter could not be determined due to lack of a concentration-response curve. The data were analyzed by comparing independent curves.

and MT$_1$-WT, and both the EC$_{50}$ (potency) and the maximal agonist-mediated response (maximal efficacy; E_{max}) were determined for βarrestin-2 recruitment and for those G proteins for which activation by MT$_1$-WT was observed: Gαi1, Gαi2, Gαi3, GαoA, GαoB, Gα12, and Gα15 (Table 1, Figure S3, and Table S3). Each signaling pathway was studied using a different biosensor, and consequently, comparison of BRET intensities can only be done between receptors for the same biosensor but not between different pathways for a same variant. Representative examples of the signaling profiles for the MT$_1$-WT, and three melatonin-responsive variants are shown in Figure 2 and clearly indicate the differential impact of variants including selective effects on the potency and/or efficacy toward the different pathways.

To provide a visual representation of the relative signaling profiles of each variant for the different signaling pathways, we used a radial graph representation including the E_{max} and the EC$_{50}$ for each pathway (Figure S4). We used a non-negative matrix factorization (NMF) and K-means clustering method to divide the variants into groups according to their functional impact similarities and differences. The different signaling profiles could be grouped in three distinct clusters. Figure 3 presents the superposition of the individual signaling profiles of each member of a given cluster providing a global view of the cluster signaling characteristics.

Cluster 1 comprises 21 variants distributed over transmembrane (TM) domains 2, 3, 4, 5, and 6, helix 8, the N-terminus (Nterm), extracellular loops (ECL) 2 and 3, and the C-terminus (Cterm) (p.G18R[Nterm], p.I88V[2.65], p.N91Y[2.68], p.G96D[3.21], p.A157V[4.55], p.G166E[4.64], p.A180T[ECL2], p.I212T[5.63], p.V221M[5.72], p.K228R[6.25], p.A266T[ECL3], p.A266V[ECL3], p.S267G[ECL3], p.R307S[8.55], p.V321M[Cterm], p.D326N[Cterm], p.V331F[Cterm], p.K334N[Cterm], p.T340I[Cterm], p.N342S[Cterm], and p.V345I[Cterm]) (superscripts represent Ballesteros−Weinstein nomenclature[24]) that did not significantly impact any of the signaling pathways considered in response to MLT. Cluster 2 comprises seven variants (p.V52A[1.57], p.R54W[1.59], p.S87L[2.64], p.H131R[3.56], p.I257F[6.54], p.I309T[8.57], and p.C314R[Cterm]) that cause a total loss of βarrestin-2 recruitment and a decrease of E_{max} and/or EC$_{50}$ for some Gα proteins, the most impacted being Gα12; however, for each of these variants, the activation of at least one G protein is not negatively impacted by the mutation. Cluster 3 comprises three variants (p.I112N[3.37], p.R125C[3.50], p.L138P[ICL2]) (intracellular loop (ICL)) with a total loss of βarrestin-2 recruitment and a global reduction in the activation of all G protein pathways.

To exclude the possibility that differences in the signaling properties, in particular EC$_{50}$ values, could result from reduced binding affinity to MLT, we determined the dissociation constant (K_d) of the melatonin receptor-specific radioligand ^{125}I-MLT for the 20 variants with decreased EC$_{50}$ values and for the melatonin-unresponsive p.P80L[2.57]. K_d values were not statistically different between the variants and the MT$_1$-WT,
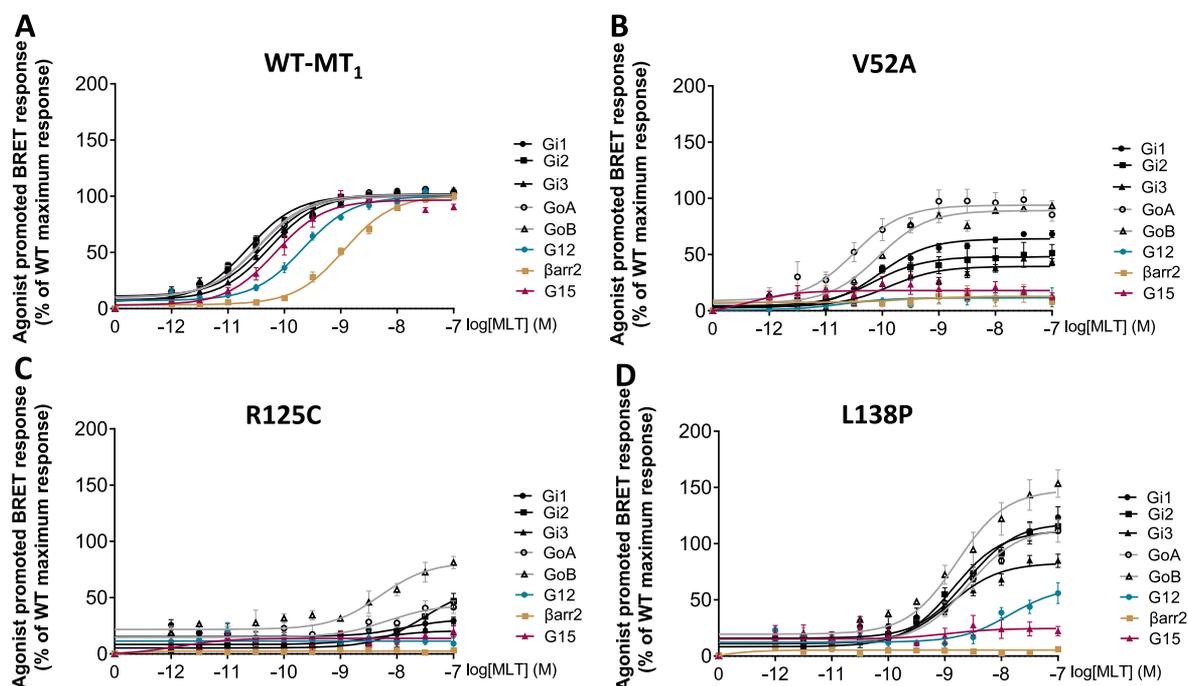
Figure 2. Melatonin concentration−response curves for G protein activations and βarrestin-2 recruitment of the MT_1-WT and representative receptor variants with distinct signaling profiles. MLT concentration curves for (A) MT_1-WT, (B) V52A, (C) R125C, and (D) L138P receptors. Data were plotted using nonlinear regression curves with a fixed Hill slope equal to 1. Data points represent means ± SEM of 14 to 16 experiments (A) or 3 to 5 experiments (B, C, D). βarr2: βarrestin-2, WT: wild-type. See also Figure S1. Data were fitted in GraphPad Prism 9.
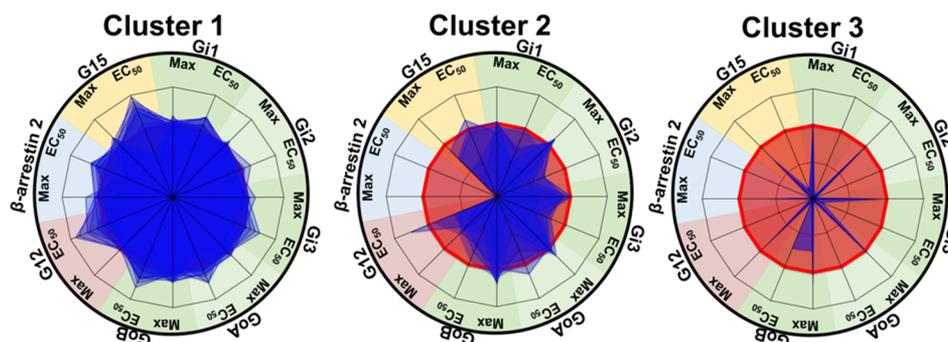
Figure 3. Radial graph representing the different variant profiles compiled in 3 clusters. Compilation of the different MT_1 variant radial graph profiles in three clusters. On each radius, maximal agonist-induced efficacy (Max) and potency (EC_{50}) are indicated. MT_1-WT profile is represented in red and mutant profiles are in blue. The values were normalized to fit a −1 to +1 scale using the following formula: (variant − WT)/(variant + WT) as indicated in the methods. A loss of potency or efficacy for a specific protein results in the decrease of the blue area. Data were fitted in Microsoft Excel 2016.

except for p.P80L[2.57], which showed a complete loss of binding capacity (Table 2). Our cell surface ELISA data show that p.P80L[2.57] expresses properly at the cell surface excluding a defect in trafficking (Figure S2). The p.P80[2.57] amino acid is part of a YPYP motif conserved in melatonin receptors. Our observation is consistent with previous studies suggesting that this motif located in transmembrane helix 2 (TM2) is crucial for both stability and activation of MT_1.[25]

Evolutionary Action Analysis of MT_1 Variants. To assess whether the extent of the functional impact of the naturally occurring variants could be estimated by the evolutionary impact of the individual substitution, we scored the Evolutionary Action (EA) of the nonsynonymous variants. EA is a bioinformatics algorithm designed to predict the impact of mutational variants[26] in which the EA score varies from 0, for variations with the most benign impact, to 100, for

those with the most adverse effects. As expected, cluster 1 is comprised of variants of low EA scores, cluster 2 of medium scores, and cluster 3 of high scores. Figure 4 shows the statistically significant correlation (R^2 = 0.580, $P < 0.0001$) between EA scores and the experimentally determined signaling phenotypic impact for each of the variants, indicating that the severity of the functional outcome of SNPs can be reasonably well predicted using trace evolution-based methods such as EA.

Structural Determinants of the Functional Impact of MT_1 Variations. To investigate the structural basis of the functional impact of the MT_1 variants, we analyzed the position and topology of the individual mutated residues of Clusters 1−3 on the three-dimensional models of the active form of MT_1 coupled to Gαi or βarrestin-2 (see Methods).

Table 2. MT$_1$ Variant Receptors Bind to Melatonin as well as the MT$_1$-WT Except P80L[a]

receptors	K_d (pM) ± SEM
Wild Type	101 ± 9.3
V52A	99 ± 6.9
R54W	178 ± 25
P80L	No binding
S87L	136 ± 19
I88V	79 ± 4.5
G96D	81 ± 8.7
I112N	244 ± 75
R125C	227 ± 61
H131R	62 ± 11
L138P	171 ± 61
G166E	63 ± 1.2
I212T	101 ± 5.0
I257F	168 ± 7.2
A266V	224 ± 43
S267G	186 ± 54
R307S	40 ± 2.5
I309T	75 ± 5.6
C314R	48 ± 7.8
K334N	395 ± 68
N342S	140 ± 43
V345I	69 ± 1.8

[a]Melatonin dissociation constant measured by 2-(^{125}I)Iodomelatonin binding experiment on MT$_1$ variants with at least one signaling defect. Data represents means ± SEM of at least three experiments.

Variants in Cluster 1 (with no impact on the receptor signaling profile) are spread throughout the structure (Figure 5A,B), appearing mostly at the surface of the extra- and intracellular domains and generally far from the ligand-binding pocket[25,27] or from any of the known GPCR activation microswitches.

The seven variants in Cluster 2 (p.V52A$^{1.57}$, p.R54W$^{1.59}$, p.S87L$^{2.64}$, p.H131R$^{3.56}$, p.I257F$^{6.54}$, p.I309T$^{8.57}$, and p.C314R^{Cterm}) are associated with a total loss of βarrestin-2 recruitment and a decrease of different Gα activations, especially for Gα12 and/or Gα15 E_{max} (Table 1 and Figure S3), but at least one Gα protein is not impacted. Interestingly, four of these variants are located at the interface between the

cytoplasmic side of TM1 (p.V52A$^{1.57}$ and p.R54W$^{1.59}$) and helix 8 (H8) (p.I309T$^{8.57}$ and p.C314R^{Cterm}) (Figure 5C). The short amphipathic H8 lies adjacent to the inner leaflet of the plasma membrane, anchored through a palmitoylated cysteine (p.C314 in MT$_1$). In other GPCRs, H8 has been shown to play a crucial role in the interaction of the receptor with βarrestin-2—leading to receptor internalization[28] and its palmitoylation has been shown to enhance the recruitment of βarrestin-2.[29] The structural models show that both H8 and ICL1 of MT$_1$ can interact with the finger loop of βarrestin-2 (Figure 5C). Thus, we hypothesize that p.V52A$^{1.57}$, p.R54W$^{1.59}$, p.I309T$^{8.57}$, and p.C314R^{Cterm} variants affect βarrestin-2 recruitment by altering the local environment of H8 in MT$_1$. Both p.I309T$^{8.57}$ and p.C314R^{Cterm} affect directly H8 by weakening hydrophobic interactions with nearby phospholipids or by removing the palmitoylation site, respectively. On the other hand, p.V52A$^{1.57}$ and p.R54W$^{1.59}$—located at the interface between TM1 and ICL1—would affect H8 indirectly. These results are consistent with findings on other GPCRs; for instance, hydrophobic amino acids in H8 of the mouse odorant receptor mOR-S6 have been suggested to form a hydrophobic core with TM1 responsible for the proper positioning of H8, and mutations of these residues increase the flexibility of H8 and destabilize its structure.[30] Not surprisingly, the loss of βarrestin-2 recruitment by these variants leads to a loss of internalization of the receptor (Figure S5) as measured by ebBRET between the RlucII-fused receptors and rGFP located in early endosomes[20] In addition, in Cluster 2, the p.H131R$^{3.56}$ variant is located at the interface between the cytoplasmic end of TM3 and ICL2, at a location where it could interact directly with βarrestin-2 (Figure 5C). This variation also places a positively charged residue next to the highly conserved p.Y126$^{3.51}$, which might alter its function by establishing a spurious cation–π interaction. Interestingly, this region has been proposed to be a secondary site for βarrestin interaction in other GPCRs.[31,32] The p.I257F$^{6.54}$ variant is located at the extracellular side of TM6 (Figure 5C), a site already shown to be important for the active melatonin-bound form of MT$_1$, favoring the conformational changes necessary for signal transmission.[33] Clement et al. proposed that, similarly to rhodopsin,[34] ECL2 of MT$_1$ stabilizes TM5, TM6, and TM7 upon activation, particularly through the interaction between ECL2 and p.I257$^{6.54}$. Consequently, we suggest that the
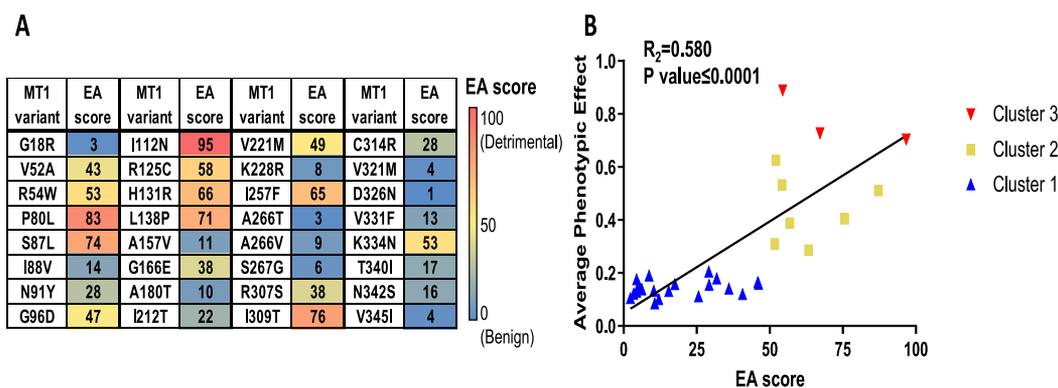

Figure 4. Evolutionary action of MT$_1$ variants and correlation with signaling impairment. (A) An evolutionary action (EA) score was calculated for each variant. EA ranges from 0 to 100 with a score of 0 predicted to be benign and a score of 100 predicted to be highly impactful or detrimental to protein function. Scores are colored based on EA (EA = 0 (blue) to EA = 100 (red)). (B) Functional defects of every MT$_1$ variant were correlated with the EA score. The 3 clusters were represented with the cluster 1 in blue, the cluster 2 in yellow, and the cluster 3 in red. Data were fitted in GraphPad Prism 9 by linear regression analysis, P and R^2 values obtained for the overall correlation.
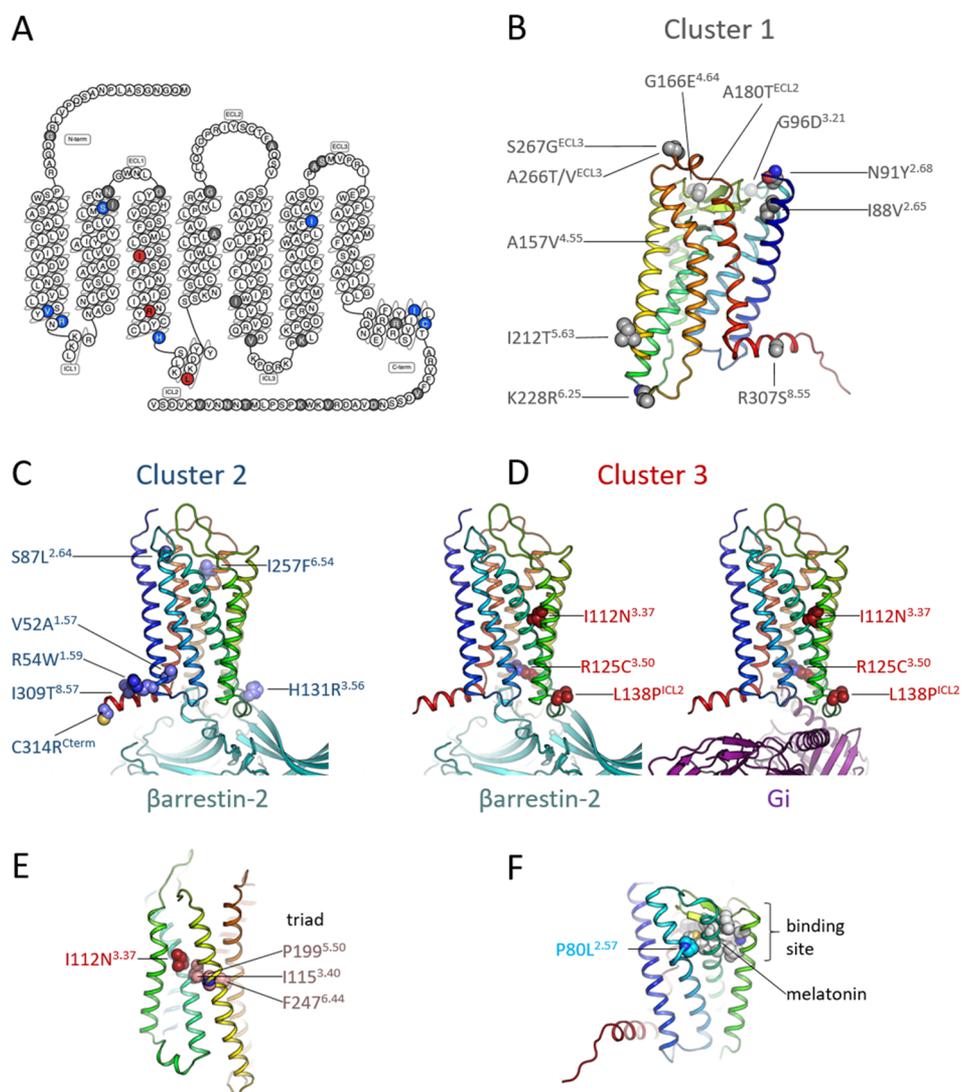
Figure 5. Location of the mutated residues and topology of Clusters 1−3. (A) Distribution of the mutated residues depicted in a 2D snake plot of the MT$_1$ receptor. Residues in Cluster 1 are colored gray, in Cluster 2 blue, and in Cluster 3 red; these colors are preserved in all panels. (B) Location of Cluster 1 mutations in the three-dimensional structure of inactive MT$_1$. The receptor is colored in a rainbow spectrum (TM1 blue - TM7/helix8 red). (C) Location of Cluster 2 mutations in active MT$_1$ bound to βarrestin-2. (D) Location of Cluster 3 mutations in active MT$_1$ bound to βarrestin-2 and Gα. (E) Mutation I112N$^{3.37}$ is located near the key functional PIF (or triad) motif. (F) Mutation P80L$^{2.57}$ is located near the binding site (shown as gray spheres) of melatonin (shown as sticks).

variation p.I257F$^{6.54}$ alters the interactions with ECL2 decreasing the stability of the MT$_1$ active form. Furthermore, p.I257$^{6.54}$ is located one turn above the highly conserved proline-kink at p.P253$^{6.50}$, a key residue in shaping TM6. The extracellular sides of TM6 and TM7—near position p.I257$^{6.54}$—form important interactions to maintain the fold of the receptor,[35] and TM7 is known to be important for the interaction between GPCRs and βarrestin.[36] Thus, the p.I257F$^{6.54}$ variant might also destabilize the TM6/7 interface and prevent the appropriate location of TM7 impairing interactions between MT$_1$ and βarrestin-2. The last variant (p.S87L$^{2.64}$) of Cluster 2 is located away from known potential functional sites (Figure 5C), which makes it difficult to rationalize its effect from a structural point of view.

We propose that residues from Cluster 2 contribute to an allosteric network between the binding pocket and the domains involved in the engagement of βarrestin-2. The fact that these variations do not affect the efficacy or potency of MT$_1$ to activate Gαi/o family members rules out the possibility

that the functional defects result from a more general misfolding of the receptor. Regarding this specific loss of βarrestin-2 recruitment and Gα12 and/or Gα15 activation, we cannot exclude the possibility that a modest nonspecific structural impairment has a more important impact on the pathways that are less efficiently coupled to the receptor. Indeed, the lower potency of MT$_1$ to activate Gα12 and Gα15 vs the Gαi/o family members suggests that these pathways are indeed less efficiently coupled to the receptor.

The burden of the seven variants of Cluster 2 were not found to be associated with an increased risk of type 2 diabetes or obesity (Table S1 and Table S2).

The three variants of Cluster 3 (p.I112N$^{3.37}$, p.R125C$^{3.50}$, and p.L138P^{ICL2}) (Figure 5D) have a more severe effect on the signaling profile of MT$_1$. On one hand, as in Cluster 2, they completely abolish βarrestin-2 recruitment (Figure S1), but moreover, they result in loss of potency (EC$_{50}$)—but not in efficacy (E$_{max}$) for p.I112N$^{3.37}$ and p.L138P^{ICL2}—in all signaling pathways compared to MT$_1$-WT. The possibility

that this loss of potency could be due to a loss of binding affinity for MLT could be ruled out, since we observe no difference in binding affinity for these three variants compared to MT_1-WT (Table 2). We suggest instead, that these variants lead to a destabilized active state and, thus, to a less efficient activation.

The variant p.L138P^{ICL2} of cluster 3 is located in ICL2, which forms a short α-helix in several GPCRs when activated that can then interact with G proteins[37] and βarrestins (Figure 5D). The exchange of a leucine for a proline is expected to either disrupt the α-helix or at least prevent an optimal position, which would lead to a less efficient interaction with G proteins and βarrestin-2 and the observed decrease in potency.

The variant p.I112N$^{3.37}$ is located in the middle of TM3 (Figure 5E) near residues p.I115$^{3.40}$ and p.P199$^{5.50}$, which are part of a key switch (the "triad" or PIF motif) for GPCR activation.[38] The p.I112N$^{3.37}$ variant would alter the packing and physicochemical properties of this region, leading to a less efficient activation of the PIF motif and an impaired transduction of the conformational changes through TM6 and TM5 that lead to the formation of the active state. As in p.L138P^{ICL2}, the p.I112N$^{3.37}$ variant can still activate G proteins (its E_{max} is unaffected), but these events are less efficient most likely due to an impaired conformational change in TM5 and TM6 leading to the observed decrease in potency.

The p.R125C$^{3.50}$ variant (Figure 5D) changes a key residue of the D/NRY motif, known to be essential for GPCR function and which is the only natural variants directly involved in the binding of βarrestins and G proteins. The p.R125C$^{3.50}$ variant shows a total loss of signaling capacity, except for GαoB which remains well activated by this variant, an observation that remains without explanation at the current state.

The burden of the three variants of Cluster 3 were not associated with an increased risk of type 2 diabetes or obesity (Table S2). The p.P80L$^{2.57}$ variant, with a completely impaired MLT binding (Figure 5F), is located in the YPYP motif (residues p.Y79$^{2.56}$ to p.P82$^{2.59}$) that shapes the ligand binding pocket by modulating a kink in TM2.[25,39] Thus, the proline to leucine substitution most likely modifies the local structure of TM2 and disrupts the binding pocket, leading to its inability to bind MLT. This variant was very rare in the Genome Aggregation Database (gnomAD; v2.1.1) with a MAF below 0.00005 and was found in a normal-glucose, obese individual from the present study.

■ DISCUSSION

Here, we took advantage of the large diversity of naturally selected variants in the coding region of the human *MTNR1A* gene encoding the MT_1 receptor to obtain mechanistic insights into the function of this receptor. Notably, all impactful mutants show a loss-of-function phenotype, and no gain of function for the pathways engaged by the WT receptor was observed. The possible gain of function for the pathways not engaged by the WT receptor was not assessed. One mutant, p.P80L$^{2.57}$, was a complete loss-of-function mutant as it could not bind MLT. Based on the functional profiles of the MLT-responsive mutants, their location in the MT_1 structure, and the general knowledge about the role of specific regions in receptor function, we were able to classify these impactful natural variants into two categories: those with severely impaired overall signaling locating near regions identified as key regions of general GPCR activation and those with major defects on more specific signaling functions, i.e., βarrestin-2

recruitment, that are located in distinct regions of ICLs and H8.

Our study reports the first exhaustive characterization of the G protein activation profile of the MT_1 receptor. Upon MLT stimulation, this receptor can activate a broad set of G proteins (Gαi1, Gαi2, Gαi3, GαoA, GαoB, Gα12, and Gα15) in addition to the recruitment of βarrestin-2 in transfected HEK293 cells. These results are consistent with the notion that MT_1 inhibits cyclic adenosine monophosphate (cAMP) production through pertussis-toxin-sensitive G proteins.[40] Here, we provide direct evidence for the ability of MT_1 to engage the entire family of Gαi/o proteins. We also show that in the Gαq/11 family only Gα15 (but not Gαq or Gα11) can be directly activated. Notably, Gα15 is an atypical member of the Gαq/11 family that has been found to be activated by a large number of GPCRs.[41] The lack of observed coupling to Gαq and Gα11 is not due to a lack of sensitivity of the biosensors or the HEK293 cells used, since coupling to more conventional Gαq/11 family members (Gαq and Gα11) can be measured in HEK293 cells for other GPCRs.[42,43] Coupling of MT_1 to Gα15 is likely to be of physiological relevance as MT_1 expression has been reported in Gα15-expressing lymphocytes in which MLT promotes diacylglycerol production.[44] MLT-promoted activation of Gα15 appears to be specific to MT_1, as it was not observed for MT_2 in our previous study using the same biosensors.[5] However, given the high sequence similarity between MT_1 and MT_2 for cluster 2 residues, no conclusion on the determinants of Gα12 and Gα15 coupling could be drawn. Our study also reveals for the first time the coupling of MT_1 to Gα12, a G protein linked to the activation of small G proteins of the Rho family and cytoskeleton modulation. Coupling to Gα12 appears to be specific to MT_1, as it was also not observed for MT_2.[5] Coupling of MT_1 to Gα12 is consistent with previous studies reporting cytoskeleton changes upon stimulation of MT_1.[45] In conclusion, our study shows that MT_1 couples not only to Gαi/o proteins, like MT_2, but shows a more expended profile by coupling in addition to Gα12 and Gα15 proteins.

Previous reports showed that frequent and rare variants in the *MTNR1B* gene encoding the MT_2 melatonin receptor are associated with type 2 diabetes (T2D) risk.[23] The most extensively studied frequent rs10830963 variant, located in the unique intron, affects insulin secretion, most likely during the development of prediabetic fasting hyperglycemia.[46] Carriers of a rare variant, located in the coding region, display a number of adverse sleep, circadian, and caloric intake phenotypes that might participate in their T2D risk.[47] We therefore evaluated whether the genetic MT_1 variants identified in our cohort of 8687 Europeans could be associated with increased risks of T2D or obesity. We were unable to detect any association either in children or in adults. The absence of association with obesity is consistent with previous observations that did not find strong support for a major role of MLT in body weight regulation and lipid metabolism in adult humans.[46] They are contrasting with rodent data showing that MLT has a beneficial effect on body weight regulation by limiting body weight gain and adipose tissue mass[48] as well as the phenotype of MT_1 knockout mice that develop selective leptin resistance in the arcuate nucleus, an important hypothalamic center for body weight control.[49] Studies in rodents indicate also a general beneficial role of melatonin on glucose homeostasis[49] and MT_1 knockout mice show systemic insulin resistance, most likely because of decreased insulin sensitivity and impaired

hepatic glucose production.[50,51] There exists some information in humans supporting the beneficial role of melatonin on glucose regulation, but the role of MT_1 remains unknown (see ref 46 for review). Our data on nonsynonymous *MTNR1A* gene variants or on genetically loss-of-function variants (i.e., p.W93*, p.Y170*, c.184 + 1G > T, c.999_1014del/p.W333*; Table S2) do not support a major role of MT_1 in T2D development. Further studies, including copy number variations, will be necessary to fully address this point, as the *MTNR1A* gene shows an exceptionally high number of gene duplications compared to other GPCR genes.[2] In conclusion, these observations indicate important species-specific differences concerning the role of MT_1 in T2D and obesity development between humans and rodents. Existing data are compatible with nonredundant functions of both MLT receptors in humans with a predominant role of MT_2 in the regulation in glucose homeostasis. Whether the variants significantly impacting G protein signaling and/or βarrestin recruitment could be associated with specific phenotypes in humans remains to be determined.

The signaling profiles obtained for 31 naturally occurring MT_1 variants reveals different signaling signatures that allowed us to classify them in three different clusters: Cluster 1 with no effect in the signaling profiles; Cluster 2 showing a major reduction in βarrestin-2 recruitment and different Gα protein activations, in particular Gα12 and/or Gα15; and Cluster 3 with severe impairing of overall signaling. Interestingly, EA scores matched the experimental results, which cross-validates the measured signaling profiles and the predictive power of evolutionary-based approaches.

The analysis of the location of these different clusters in three-dimensional structural models of active MT_1 allowed us to propose specific mechanisms for the effect of the variations on receptor activation and signaling. The effects in Cluster 2 can be explained in most of the cases by alterations in the structure/dynamics of H8 that impair receptor-βarrestin-2 interactions. On the other hand, each variant in Cluster 3 is located near key regions for GPCR activation (the helical ICL2, the D/NRY motif, and the PIF motif); these variations may thus alter the signaling profile by altering the environment of these activation switches and impairing their function.

Interestingly, we found specific mutations that have a greater impact on βarrestin-2 recruitment, exemplifying how distinct receptor domains and allosteric interaction networks are involved in functional selectivity, i.e., the selective engagement of distinct signaling pathways. Remarkably, we found natural MT_1 variants with signaling defects in apparently healthy people. However, the lack of detectable disease association may be due to the rare frequency of the variants that prevent robust statistical analysis. Alternatively, as MLT can act through two receptors—MT_1 and MT_2—one could think that MT_2 could compensate for any loss of MT_1 activity. However, it has been recently shown that MT_2 can only activate Gαi/o family members and to recruit βarrestin-2.[5] Thus, such compensation from MT_2 would only lead to partial signaling in response to MLT production. Most striking defects would be expected in individuals carrying MT_1 defective variants in those cells/tissues in which MT_2 is unable to compensate the MT_1 defect, either because of the absence of MT_2 expression or because of a MT_1-specific function. Prominent examples are lymphocytes and MCF-7 human breast cancer cells, both expressing exclusively MT_1 receptors. In addition, differential roles of MT_1 and MT_2 in sleep and

circadian rhythm regulation have been suggested.[16] Based on our observation that several variant carriers show a complete loss of βarrestin-2 recruitment to MT_1, the study of such variants in these biological system should be informative on the role of MT_1-mediated βarrestin-2 signaling.

In conclusion, we have shown that sequencing and the functional characterization of rare variants combined to their computational analysis in relation with structural modeling represent valuable tools to identify key functional regions or residues in a receptor and allow prediction and rationalization of the effect of mutations on functional selectivity.

■ METHODS

Study Participants. We investigated 8687 blood DNA samples from several population studies: (1) 3443 participants from the D.E.S.I.R. 9-year prospective study including middle-aged men and women from western France;[52] (2) 2642 participants who were recruited and followed up either by the CNRS UMR8199 (Lille, France), by the Department of Nutrition of Hotel-Dieu Hospital (Paris, France), or by the Centre d'Etude du Polymorphisme Humain (CEPH, Saint-Louis Hospital, Paris, France);[53,54] (3) 1567 participants who were recruited from the Department of Endocrinology of the Corbeil-Essonnes Hospital (Corbeil-Essonnes, France);[53] (4) 631 participants from the French Haguenau regional cohort study;[55] (5) 404 participants from the French Fleurbaix-Laventie Ville Santé study.[56] The study protocols were approved by local ethics committees. All participants older than 18 years signed an informed consent form. Oral assent from children or adolescents was obtained and parents (or legal guardian) signed an informed consent form.

In participants older than 18 years, obesity was defined as body mass index (BMI) $\geq$ 30 kg.m^{-2}, while normal weight was defined as BMI < 25 kg.m^{-2}. In children and adolescents younger than 18 years old, obesity was defined as BMI-for-age $\geq$95th percentile, while normal weight was defined as BMI-for-age <85th percentile according to the Centers for Disease Control and Prevention (CDC) growth charts. Type 2 diabetes (T2D) was defined as fasting plasma glucose $\geq$7.0 mmol L^{-1}, and/or use of hyperglycemia treatment; while normal glucose was defined as fasting plasma glucose <6.1 mmol L^{-1} without hyperglycemia treatment.

Next-Generation Sequencing, Detection of *MTNR1A* Coding Variants, and Their Association Analyses. NGS targeting the coding exons of *MTNR1A* (NM_005958.4) was done as previously described.[57] In brief, target enrichment was performed according to the manufacturer's protocol (NimbleGen SeqCap EZ) for Illumina sequencing. Sequence reads were mapped to the human genome (hg19/GRCh37) using Burrows-Wheeler Aligner (version 0.7.13). The variant calling was performed using Genome Analysis ToolKit (GATK; version 3.3). The annotation of variants was performed using the Ensembl Perl Application Program Interfaces (version 75). In the participants, all *MTNR1A* coding variants had a coverage higher than 8 reads and a QUAL score higher than 50. No variant had more than 5% of missing genotype (i.e., with a depth of coverage below 8 reads or a QUAL score below 50) across the participants, and no participant had more than 5% of missing genotypes (i.e., with a depth of coverage below 8 reads or a QUAL score below 50) across *MTNR1A*. The location of each variant was determined relative to the translation initiation codon using Human Genome Variation Society (HGVS) nomenclature for the description of variants.

Among adults, we performed a case-control study for obesity adjusted for age, sex, the presence of T2D and genetic ancestry (controls were normal-weight adults), and a case-control study for T2D adjusted for age, sex, BMI, and genetic ancestry (controls were normal glucose adults with age above 40). Among children and adolescents, we performed a case-control study for obesity adjusted for age and sex (controls were normal-weight children/adolescents). Ancestry assessment was done as previously described.[57] The rare variants (with a MAF below 1%) were analyzed as a single cluster using MiST. MiST provides a score statistic $S(\pi)$ for the mean effect (π) of the cluster, and a score statistic $S(\tau)$ for the heterogeneous effect (τ) of the cluster. The overall p-value is the combined p-values P_π and P_τ from the Fisher's procedure. The frequent variants (with a MAF above 1%) were separately analyzed using a standard logistic regression adjusted for covariates defined above.

Cell Culture and Transfection. HEK293T cells were grown in complete medium (Dulbecco's modified Eagle's medium supplemented with 10% fetal bovine serum, 4.5 g·L^{-1} glucose, 100 U mL^{-1} penicillin, 0.1 mg mL^{-1} streptomycin, and 1 mM glutamine) (Invitrogen, CA). Transient transfections were performed using PEI (Sigma-Aldrich), according to manufacturer's instructions.

Analysis of Cell Surface Receptor Expression. ELISAs were performed using the mouse antiflag antibody (Sigma-Aldrich, cat# F3165, RRID: AB_259529) and a horseradish peroxidase-conjugated mouse immunoglobulin G (IgG) whole-sheep secondary antibody (Sigma-Aldrich, cat# A6782, RRID: AB_258315).

Bioluminescence Resonance Energy Transfer (BRET) Measurement. Gαi1/i2/i3/oA/oB activations was assessed by measuring change of BRET between RlucII-Gαi1/i2/i3/oA/oB and GFP10-Gγ2 upon treatment of HEK293 cells cotransfected to express receptor and BRET sensors with MLT (Sigma-Aldrich).[5,19] For RlucII-Gαs, RlucII-Gαz, RlucII-Gαq, and RlucII-Gα12, we used the appropriate RlucII-tagged Gα subunits,[5] GFP10-Gγ1 was used given that optimal responsive window is generally obtained using these BRET sensor pairs for these Gα proteins. In all cases, the BRET pairs were used in the presence of untagged Gβ1 protein. Gα15 activation by receptors was assessed using a unimolecular biosensor. Since MT$_1$ stimulation by melatonin does not activate PKC in our HEK293T cells in the absence of Gα15 but does so in its presence, we used the PKC activation as a surrogate assay to measure Gα15 activation by MT$_1$. PKC activation was assessed by measuring BRET with this unimolecular biosensor. The BRET2-based PKC sensor consists of GFP10, 2 phospho-sensing domains (FHA1 and FHA2), a long and flexible linker, 2 specific phospho-substrate sequences, a RlucII, and the diacyl glycerol (DAG)-binding "C1b" domain of PKCδ added to increase signal specificity. Once phosphorylated, the phospho-substrates interact with their respective phospho-sensing domain, which stabilizes a conformation characterized by a higher BRET signal. βarrestin-2 recruitment was assessed by measuring BRET between RlucII-βarrestin-2 and rGFP-CAAX (prenylation CAAX box of KRas) demonstrating the recruitment of the βarrestin-2 to the plasma membrane.[20] Transfected cells were plated in 96-well white microplates (100 μL per well; Greiner). Forty-eight hours after transfection, cells were washed with Dulbecco's phosphate-buffered saline, and then Tyrode's buffer was added. After the addition of MLT, the cells were incubated for 10 min at 37 °C, and

coelenterazine 400a (2.5 μM; NanoLight Technology) was added 5 min before BRET reading in a Synergy Neo Microplate reader (BioTek) (acceptor filter: 515 ± 15 nm; donor filter: 410 ± 40 nm).

To monitor receptor internalization, ebBRET was measured between MT$_1$-WT or variants (R54W, I309T, or C314R) fused to RlucII and the endosomal compartment marker rGFP-FYVE.[20] Prolume purple (2.5 μM; NanoLight Technology) is added for 6 min followed by MLT stimulation and readings are recorded on a Mithras (Berthold scientific) microplate reader (acceptor filter: 515 ± 10 nm; donor filter: 400 ± 35 nm).

Net BRET represents the BRET signal minus the signal in the absence of a GFP10-tagged sensor. ΔBRET refers to the difference in net BRET recorded from cells treated with agonist and cells treated with vehicle. For the agonist concentration−response curves, the responses for the variants were expressed as a % of the response observed for the WT receptor.

Evolutionary Action. The evolutionary action (EA) of a mutation on fitness is given by[26]

$$\mathrm{d}\phi = \nabla f \cdot \mathrm{d}\gamma \tag{1}$$

where ϕ is the fitness phenotype, γ is the genotype sequence, and f is the evolutionary function between them: $f(\gamma) = \phi$. Although the function f describes the fitness landscape and is unknown, its derivative is formally given by eq 1, the terms of which can be approximated from evolutionary information. Specifically, $\mathrm{d}y$ is the magnitude of mutation, which can be calculated in terms of log odds of amino acid substitutions in the case of a coding mutation, and ∇f is the gradient of the fitness landscape, which can be calculated from the functional sensitivity to mutations at each sequence positions, which can be calculated by the coupling between sequence variations and phylogenetic divergences.[58] In practice, the EA score is normalized by percentile rank from 0 to 100, where a variant is relatively more deleterious as the score close to 100. This approach tends to perform well against other predictors of variant effect in blind challenges.[59] To predict the effect of each variant within the MT$_1$ receptor, EA score is calculated using *MTNR1A* multiple sequence alignment retrieved from the nonredundant protein sequence (nr) database (https://blast.ncbi.nlm.nih.gov/Blast.cgi).

Statistical Analysis of Functional Analyses. Data are presented as means ± SEM of indicated "n" independent experiments, performed at least in triplicate to ensure the reliability of single values. The level of probability used in this article is defined as follows: NS: nonsignificant, *$p < 0.05$, **$p < 0.01$, ***$p < 0.001$ relative to control.

LogEC$_{50}$ and agonist-induced $E_{\max}$ values were obtained following nonlinear regression (curve fit) with four parameters of data from a minimum of eight different concentrations per experiment, repeated at least three times independently. All assays performed in this study were previously validated and demonstrated the robustness and variability of the procedure using this number of independent experiments for concentration−response curves. Data and statistical analysis were performed using GraphPad Prism software version 6.0.

For each assay, the agonist-induced $E_{\max}$ value for every MT$_1$ variant was normalized as a percentage of the maximal MLT-stimulated response of the WT receptor (set at 100) monitored in parallel with the receptor variant. The dose−response curves were fitted to an operational model of agonism designed by Kenakin and Christopoulos[60,61] to obtain log(τ/

KA) values for the WT receptor and its variants. Normally, an agonist is set as a reference agonist, against which within-pathway comparisons for the same receptor to other agonists can be made and expressed as $\Delta\log(\tau/KA)$. Here, within-pathway comparisons were made between MT_1 variants and the WT receptor. Normalized difference was calculated on values corresponding to agonist-induced E_{max}, and $\log EC_{50}$ to fit a -1 to $+1$ scale using the following formula: (variant − WT)/(variant + WT). In the case of $\log EC_{50}$, before normalization, the antilogs were first calculated and then were fitted to the aforementioned formula. Positive and negative values represent mutations with better or worse responses, respectively, than those of the WT receptor. Subsequently, $\log EC_{50}$, agonist-induced E_{max}, and $\Delta\log(\tau/KA)$ values were expressed as means ± SEM of the indicated number of experiments (n). Statistical analysis for $\log EC_{50}$ and agonist-induced E_{max} was performed by comparing independent fits with a global fit that shared the selected parameter.

Computational Analysis. To quantify similarities between signaling perturbations resulting from each mutation, we adapted the NMF and K-means clustering process originally described in ref 6. We performed this analysis on an input matrix of 31 mutations and 24 signaling parameters spanning 8 signaling pathways ($G\alpha i1/G\alpha i2/G\alpha i3/G\alpha oA/G\alpha oB/G\alpha 12/G\alpha 15/\beta$arrestin-2) in response to melatonin. The mean and STD for each phenotypic measure were used to propagate experimental error through the clustering process. Explicitly, 1000 input matrices were generated by independently sampling from the experimental error (Mean + STD) for each phenotypic data point. Each of these sampled input matrices were then processed separately using the NMF/K-means method. The values for each phenotype were scaled to avoid bias introduced by differences in phenotype scale using

Standardized value
$$= (X_{ij} - \text{minimum}_j)/(\text{maximum}_j - \text{minimum}_j)$$

for every mutation i and every parameter j, where maximum_j and minimum_j values were specific to each parameter column (e.g., EC_{50}, E_{max}, τ/Ka). In this way, every parameter was normalized between 0 and 1. The dimensionality of these 1000 input matrices were then independently reduced using NMF to identify the key signaling patterns. K-means clustering was used, as described, to cluster the [mutation × feature] (31 × K) basis vector. As previously described, clustering results for each sampled matrix were averaged across $K = 2$ to $K = 6$, where K is the number of features for NMF and the number of clusters for K-means ($K_{NMF} = K_{K-means}$). Final cluster assignment, quantifying mutation similarity, was the average over all 1000 sampled matrices. Clustering frequency was converted into distance matrix using Pearson's correlation and visualized as a heatmap and dendrogram.

Radioligand Binding Experiments. Radioligand saturation binding experiments were performed in transient transfected HEK293T cell lines. Saturation binding assays were carried out on crude membrane preparations with increasing concentrations of 2-[^{125}I]MLT (PerkinElmer Life Sciences) to determine dissociation constants (K_d) and total melatonin receptor expression (B_{max}) of wild-type and mutant MT_1 receptors using PRISM software (GraphPad). Non-specific binding was determined using 10 μM melatonin.

Three-Dimensional Modeling. The location of the mutant variants in the inactive state of MT_1 was mapped onto the crystal structure of MT_1 bound to ramelteon (PDBid: 6ME2).[25] The location of the mutant variants in the active state of MT_1 was mapped onto a three-dimensional model of the receptor built by homology modeling using as templates (i) the cryo-EM structure of the human mu-opioid receptor (33% sequence similarity) in complex with $G\alpha i$ (PDBid: 6DDE)[62] for the transmembrane bundle (TM1−TM7; residues 21−290), and (ii) the crystal structure of the human adenosine A2A receptor (26% sequence similarity) (PDBid: 2YDO)[63] for the last 18 residues of the model comprising ICL4 and helix 8 (residues 291−308). We chose A2A receptor as a template because, although it couples to $G\alpha s$, it has a high sequence similarity with MT_1 in the transmembrane domain (see above) and, importantly, is phylogenetically close to it (the melatonin receptor cluster and the MECA receptor cluster are neighbors in the α group of class A GPCRs[64]). A structure-based sequence alignment between the templates and MT_1 was obtained from the GPCRdb.[65] This initial alignment was manually refined using Chimera[66] to adjust the gaps in the loop regions. Using this alignment and the structural templates, 3D models of MT_1 in an active conformations were built using Modeler ver. 9.16.[67] The cysteine bridge between p.C100$^{3.25}$ in TM3 and p.C177$^{ecl2.50}$ in the second ECL was explicitly defined during model building. All models were subjected to 300 iterations of variable target function method (VTFM) optimization and thorough ($md\_level = refine.slow$) molecular dynamics and simulated annealing optimization within Modeler, and scored using the discrete optimized protein energy potential.[67] The 20 best-scoring models were analyzed visually, and a suitable model (in term of low score and structure of the loops) was selected.

To visualize the arrangement of the $MT_1/G\alpha i$ and $MT_1/$arrestin complexes, the structures of $G\alpha i$ (PDBid: 6DDE)[62] and visual βarrestin-1 (PDBid: 5W0P)[68] were structurally aligned onto the model of active MT_1 (using the receptor transmembrane domains for the fit) with molecular graphics software (The PyMOL Molecular Graphics System, Version 2.2.3, Schrödinger, LLC.).

■ ASSOCIATED CONTENT

ⓢ Supporting Information

The Supporting Information is available free of charge at https://pubs.acs.org/doi/10.1021/acsptsci.1c00157.

> BRET-based biosensors used (Figures S1), cell surface expression of MT_1 variants (Figure S2), concentration−response curve and radial graph of MT_1 variants grouped in 3 clusters (Figure S3−S4), kinetics of MT_1 internalization (Figure S5), functional characterization and association of *MTNR1A* coding variants to diabetes or obesity (Tables S1−S3) PDF)

■ AUTHOR INFORMATION

Corresponding Authors

Ralf Jockers − *Université de Paris, Institut Cochin, CNRS, INSERM, F-75014 Paris, France;* ⓞ orcid.org/0000-0002-4354-1750; Email: ralf.jockers@inserm.fr

Michel Bouvier − *Department of Biochemistry and Molecular Medicine, University de Montréal, Montreal, Quebec H3T 1J4, Canada; Institute for Research in Immunology and Cancer, University of Montreal, Montreal, Quebec H3T 1J4, Canada;* ⓞ orcid.org/0000-0003-1128-0100; Email: michel.bouvier@umontreal.ca

Authors

Alan Hegron — *Université de Paris, Institut Cochin, CNRS, INSERM, F-75014 Paris, France; Department of Biochemistry and Molecular Medicine, University de Montréal, Montreal, Quebec H3T 1J4, Canada; Institute for Research in Immunology and Cancer, University of Montreal, Montreal, Quebec H3T 1J4, Canada;* Present Address: Dept. of Molecular Pathobiology, New York University College of Dentistry, New York, New York 10010, United States of America

Eunna Huh — *Department of Pharmacology and Chemical Biology, Baylor College of Medicine, Houston, Texas 77030, United States of America*

Xavier Deupi — *Laboratory of Biomolecular Research and Condensed Matter Theory group, Paul Scherrer Institute (PSI), 5232 Villigen, Switzerland;* ⊙ orcid.org/0000-0003-4572-9316

Badr Sokrat — *Department of Biochemistry and Molecular Medicine, University de Montréal, Montreal, Quebec H3T 1J4, Canada; Institute for Research in Immunology and Cancer, University of Montreal, Montreal, Quebec H3T 1J4, Canada*

Wenwen Gao — *Université de Paris, Institut Cochin, CNRS, INSERM, F-75014 Paris, France*

Christian Le Gouill — *Institute for Research in Immunology and Cancer, University of Montreal, Montreal, Quebec H3T 1J4, Canada*

Mickaël Canouil — *Inserm UMR1283, CNRS UMR8199, European Genomic Institute for Diabetes (EGID), Institut Pasteur de Lille, Lille 59000, France; University of Lille, Lille University Hospital, Lille 59000, France*

Mathilde Boissel — *Inserm UMR1283, CNRS UMR8199, European Genomic Institute for Diabetes (EGID), Institut Pasteur de Lille, Lille 59000, France; University of Lille, Lille University Hospital, Lille 59000, France*

Guillaume Charpentier — *Centre d'Étude et de Recherche pour l'Intensification du Traitement du Diabète, 91000 Evry, France*

Ronan Roussel — *Department of Diabetology Endocrinology Nutrition, Hôpital Bichat, DHU FIRE, Assistance Publique Hôpitaux de Paris, 75004 Paris, France; Inserm U1138, Centre de Recherche des Cordeliers, 75006 Paris, France; UFR de Médecine, University Paris Diderot, Sorbonne Paris Cité, 75006 Paris, France*

Beverley Balkau — *Inserm U1018, Center for Research in Epidemiology and Population Health, 94805 Villejuif, France; University Paris-Saclay, University Paris-Sud, 94270 Villejuif, France*

Philippe Froguel — *Inserm UMR1283, CNRS UMR8199, European Genomic Institute for Diabetes (EGID), Institut Pasteur de Lille, Lille 59000, France; University of Lille, Lille University Hospital, Lille 59000, France; Department of Metabolism, Imperial College London, London W12 0NN, United Kingdom*

Bianca Plouffe — *Department of Biochemistry and Molecular Medicine, University de Montréal, Montreal, Quebec H3T 1J4, Canada; Institute for Research in Immunology and Cancer, University of Montreal, Montreal, Quebec H3T 1J4, Canada;* Present Address: The Wellcome-Wolfson Institute for Experimental Medicine, Queen's University Belfast, Belfast, BT9 7BL, United Kingdom; ⊙ orcid.org/0000-0002-8321-0796

Amélie Bonnefond — *Inserm UMR1283, CNRS UMR8199, European Genomic Institute for Diabetes (EGID), Institut Pasteur de Lille, Lille 59000, France; University of Lille, Lille University Hospital, Lille 59000, France; Department of Metabolism, Imperial College London, London W12 0NN, United Kingdom*

Olivier Lichtarge — *Department of Pharmacology and Chemical Biology, Baylor College of Medicine, Houston, Texas 77030, United States of America; Department of Molecular and Human Genetics, Baylor College of Medicine, Houston, Texas 77030, United States*

Complete contact information is available at:
https://pubs.acs.org/10.1021/acsptsci.1c00157

Author Contributions

AH, CLG, BP, RJ, and MBouvier conceived and designed experiments. AH and WG made constructions of variant plasmids. AH performed most of the experiments to characterize the receptors' functionality with the exception of binding done by WG. BS contributed to the BRET experiments. EH and OL did the clustering analysis. XD built and analyzed the 3D models. AB and PF conceived and designed the next-generation sequencing study and analyzed the genetic variants. MC and MBoissel performed statistical analyses related to genetic data. GC, RR, and BB contributed DNA samples from patients. AH, CLG, BP, and MBouvier analyzed data. PF, MBouvier, and RJ obtained the funding. AH, RJ, and MBouvier wrote the manuscript that was edited and/or approved by all authors.

Notes

Data availability: All data needed to evaluate the conclusions in the paper are present in the paper and/or the Supporting Information. All biosensors are available for academic non-commercial studies through regular Material Transfer Agree-

ments and can be requested by email: michel.bouvier@umontreal.ca.

Ethics approval: The study protocols were approved by local ethics committees. All participants older than 18 years signed an informed consent form. Oral assent from children or adolescents was obtained and parents (or legal guardian) signed an informed consent form.

■ ACKNOWLEDGMENTS

■ ABBREVIATIONS

GPCR, G protein-coupled receptor; NGS, next-generation sequencing; GRKs, GPCR-regulated kinases; MT_1, melatonin receptor 1; MT_2, melatonin receptor type 2; MLT, melatonin; BRET, bioluminescence resonance energy transfer; ebBRET, enhanced bystander BRET; WT, wild-type; MAF, minor allele frequency; ELISA, enzyme linked immunosorbent assay; E_{max}, maximal efficacy; NMF, non-negative matrix factorization; TM, transmembrane; Nterm, N-terminus; ECL, extracellular loops; Cterm, C-terminus; ICL, intracellular loop; K_d, dissociation constant; EA, evolutionary action; H8, helix 8; EC_{50}, potency; BMI, body mass index; CDC, Centers for Disease Control and Prevention; T2D, Type 2 diabetes; GATK, Genome Analysis ToolKit; HGVS, Human Genome Variation Society; DAG, diacyl glycerol; CAAX, prenylation CAAX box of KRas; GFP, green fluorescent protein; rGFP, *Renilla* GFP; Rluc, *Renilla* luciferase; nr, nonredundant; VTFM, variable target function method; βarr-2, βarrestin-2; HEK293 cells, human embryonic kidney 293 cells; PKC, protein kinase C; cAMP, cyclic adenosine monophosphate

■ REFERENCES

(1) Abecasis, G. R.; Altshuler, D.; Auton, A.; Brooks, L. D.; Durbin, R. M.; Gibbs, R. A.; Hurles, M. E.; McVean, G. A. A map of human genome variation from population-scale sequencing. *Nature* **2010**, *467* (7319), 1061−1073.

(2) Hauser, A. S.; Chavali, S.; Masuho, I.; Jahn, L. J.; Martemyanov, K. A.; Gloriam, D. E.; Babu, M. M. Pharmacogenomics of GPCR Drug Targets. *Cell* **2018**, *172* (1−2), 41−54.

(3) DeBoever, C.; Venkatakrishnan, A.; Paggi, J. M.; Heydenreich, F. M.; Laurin, S.-A.; Masureel, M.; Tanigawa, Y.; Venkataraman, G.; Bouvier, M.; Dror, R.; Rivas, M. A. Medical relevance of common protein-altering variants in GPCR genes across 337,205 individuals in the UK Biobank study. *bioRxiv* **2019**, 876250 DOI: 10.1101/2019.12.13.876250.

(4) DePristo, M. A.; Weinreich, D. M.; Hartl, D. L. Missense meanderings in sequence space: a biophysical view of protein evolution. *Nat. Rev. Genet.* **2005**, *6* (9), 678−687.

(5) Karamitri, A.; Plouffe, B.; Bonnefond, A.; Chen, M.; Gallion, J.; Guillaume, J. L.; Hegron, A.; Boissel, M.; Canouil, M.; Langenberg, C.; Wareham, N. J.; Le Gouill, C.; Lukasheva, V.; Lichtarge, O.; Froguel, P.; Bouvier, M.; Jockers, R. Type 2 diabetes-associated variants of the MT2 melatonin receptor affect distinct modes of signaling. *Sci. Signaling* **2018**, *11* (545), No. eaan6622.

(6) Schonegge, A. M.; Gallion, J.; Picard, L. P.; Wilkins, A. D.; Le Gouill, C.; Audet, M.; Stallaert, W.; Lohse, M. J.; Kimmel, M.; Lichtarge, O.; Bouvier, M. Evolutionary action and structural basis of the allosteric switch controlling beta2AR functional selectivity. *Nat. Commun.* **2017**, *8* (1), 2169.

(7) Zhao, D.; Yu, Y.; Shen, Y.; Liu, Q.; Zhao, Z.; Sharma, R.; Reiter, R. J. Melatonin Synthesis and Function: Evolutionary History in Animals and Plants. *Front. Endocrinol. (Lausanne, Switz.)* **2019**, *10*, 249.

(8) Jockers, R.; Delagrange, P.; Dubocovich, M. L.; Markus, R. P.; Renault, N.; Tosini, G.; Cecon, E.; Zlotos, D. P. Update on melatonin receptors: IUPHAR Review 20. *Br. J. Pharmacol.* **2016**, *173* (18), 2702−2725.

(9) Cecon, E.; Oishi, A.; Jockers, R. Melatonin receptors: molecular pharmacology and signalling in the context of system bias. *Br. J. Pharmacol.* **2018**, *175* (16), 3263−3280.

(10) Fujieda, H.; Scher, J.; Hamadanizadeh, S. A.; Wankiewicz, E.; Pang, S. F.; Brown, G. M. Dopaminergic and GABAergic amacrine cells are direct targets of melatonin: immunocytochemical study of mt1 melatonin receptor in guinea pig retina. *Vis Neurosci* **2000**, *17* (1), 63−70.

(11) Scher, J.; Wankiewicz, E.; Brown, G. M.; Fujieda, H. MT(1) melatonin receptor in the human retina: expression and localization. *Invest Ophthalmol Vis Sci.* **2002**, *43* (3), 889−897.

(12) Ng, K. Y.; Leong, M. K.; Liang, H.; Paxinos, G. Melatonin receptors: distribution in mammalian brain and their respective putative functions. *Brain Struct. Funct.* **2017**, *222* (7), 2921−2939.

(13) Guerrero, J. M.; Reiter, R. J. Melatonin-immune system relationships. *Curr. Top. Med. Chem.* **2002**, *2* (2), 167−179.

(14) Skwarlo-Sonta, K.; Majewski, P.; Markowska, M.; Oblap, R.; Olszanska, B. Bidirectional communication between the pineal gland and the immune system. *Can. J. Physiol. Pharmacol.* **2003**, *81* (4), 342−349.

(15) Dubocovich, M. L.; Hudson, R. L.; Sumaya, I. C.; Masana, M. I.; Manna, E. Effect of MT1 melatonin receptor deletion on melatonin-mediated phase shift of circadian rhythms in the C57BL/6 mouse. *J. Pineal Res.* **2005**, *39* (2), 113−120.

(16) Gobbi, G.; Comai, S. Differential Function of Melatonin MT1 and MT2 Receptors in REM and NREM Sleep. *Front. Endocrinol. (Lausanne, Switz.)* **2019**, *10*, 87.

(17) Benleulmi-Chaachoua, A.; Hegron, A.; Le Boulch, M.; Karamitri, A.; Wierzbicka, M.; Wong, V.; Stagljar, I.; Delagrange, P.; Ahmad, R.; Jockers, R. Melatonin receptors limit dopamine reuptake by regulating dopamine transporter cell-surface exposure. *Cell. Mol. Life Sci.* **2018**, *75* (23), 4357−4370.

(18) Li, C.; Qiao, B.; Zhan, Y.; Peng, W.; Chen, Z. J.; Sun, L.; Zhang, J.; Zhao, L.; Gao, Q. Association between genetic variations in MTNR1A and MTNR1B genes and gestational diabetes mellitus in Han Chinese women. *Gynecol. Obstet. Invest.* **2013**, *76* (4), 221−227.

(19) Gales, C.; Van Durm, J. J.; Schaak, S.; Pontier, S.; Percherancier, Y.; Audet, M.; Paris, H.; Bouvier, M. Probing the activation-promoted structural rearrangements in preassembled receptor-G protein complexes. *Nat. Struct. Mol. Biol.* **2006**, *13* (9), 778−786.

(20) Namkung, Y.; Le Gouill, C.; Lukashova, V.; Kobayashi, H.; Hogue, M.; Khoury, E.; Song, M.; Bouvier, M.; Laporte, S. A. Monitoring G protein-coupled receptor and beta-arrestin trafficking in live cells using enhanced bystander BRET. *Nat. Commun.* **2016**, *7*, 12178.

(21) Milligan, G.; Marshall, F.; Rees, S. G16 as a universal G protein adapter: implications for agonist screening strategies. *Trends Pharmacol. Sci.* **1996**, *17* (7), 235−237.

(22) Namkung, Y.; LeGouill, C.; Kumar, S.; Cao, Y.; Teixeira, L. B.; Lukasheva, V.; Giubilaro, J.; Simões, S. C.; Longpré, J.-M.; Devost, D.; Hébert, T. E.; Piñeyro, G.; Leduc, R.; Costa-Neto, C. M.; Bouvier, M.; Laporte, S. A. Functional selectivity profiling of the angiotensin II type 1 receptor using pathway-wide BRET signaling sensors. *Sci. Signaling* **2018**, *11* (559), No. eaat1631.

(23) Bonnefond, A.; Clement, N.; Fawcett, K.; Yengo, L.; Vaillant, E.; Guillaume, J. L.; Dechaume, A.; Payne, F.; Roussel, R.; Czernichow, S.; Hercberg, S.; Hadjadj, S.; Balkau, B.; Marre, M.; Lantieri, O.; Langenberg, C.; Bouatia-Naji, N.; Charpentier, G.; Vaxillaire, M.; Rocheleau, G.; Wareham, N. J.; Sladek, R.; McCarthy, M. I.; Dina, C.; Barroso, I.; Jockers, R.; Froguel, P. Rare MTNR1B variants impairing melatonin receptor 1B function contribute to type 2 diabetes. *Nat. Genet.* **2012**, *44* (3), 297−301 Meta-Analysis of Glucose and Insulin-Related Traits Consortium (MAGIC);.

(24) Ballesteros, J. A.; Weinstein, H., [19] Integrated methods for the construction of three-dimensional models and computational probing of structure-function relations in G protein-coupled receptors. In *Methods in neurosciences*; Elsevier: 1995; Vol. 25; pp 366−428.

(25) Stauch, B.; Johansson, L. C.; McCorvy, J. D.; Patel, N.; Han, G. W.; Huang, X. P.; Gati, C.; Batyuk, A.; Slocum, S. T.; Ishchenko, A.; Brehm, W.; White, T. A.; Michaelian, N.; Madsen, C.; Zhu, L.; Grant, T. D.; Grandner, J. M.; Shiriaeva, A.; Olsen, R. H. J.; Tribo, A. R.; Yous, S.; Stevens, R. C.; Weierstall, U.; Katritch, V.; Roth, B. L.; Liu, W.; Cherezov, V. Publisher Correction: Structural basis of ligand recognition at the human MT1 melatonin receptor. *Nature* 2019, 569 (7756), E6.

(26) Katsonis, P.; Lichtarge, O. A formal perturbation equation between genotype and phenotype determines the Evolutionary Action of protein-coding variations on fitness. *Genome Res.* 2014, 24 (12), 2050−2058.

(27) Pala, D.; Lodola, A.; Bedini, A.; Spadoni, G.; Rivara, S. Homology models of melatonin receptors: challenges and recent advances. *Int. J. Mol. Sci.* 2013, 14 (4), 8093−8121.

(28) Feierler, J.; Wirth, M.; Welte, B.; Schussler, S.; Jochum, M.; Faussner, A. Helix 8 plays a crucial role in bradykinin B(2) receptor trafficking and signaling. *J. Biol. Chem.* 2011, 286 (50), 43282−43293.

(29) Charest, P. G.; Bouvier, M. Palmitoylation of the V2 vasopressin receptor carboxyl tail enhances beta-arrestin recruitment leading to efficient receptor endocytosis and ERK1/2 activation. *J. Biol. Chem.* 2003, 278 (42), 41541−41551.

(30) Sato, T.; Kawasaki, T.; Mine, S.; Matsumura, H. Functional Role of the C-Terminal Amphipathic Helix 8 of Olfactory Receptors and Other G Protein-Coupled Receptors. *Int. J. Mol. Sci.* 2016, 17 (11), 1930.

(31) Marion, S.; Oakley, R. H.; Kim, K. M.; Caron, M. G.; Barak, L. S. A beta-arrestin binding determinant common to the second intracellular loops of rhodopsin family G protein-coupled receptors. *J. Biol. Chem.* 2006, 281 (5), 2932−2938.

(32) Raman, D.; Osawa, S.; Gurevich, V. V.; Weiss, E. R. The interaction with the cytoplasmic loops of rhodopsin plays a crucial role in arrestin activation and binding. *J. Neurochem.* 2003, 84 (5), 1040−1050.

(33) Clement, N.; Renault, N.; Guillaume, J. L.; Cecon, E.; Journe, A. S.; Laurent, X.; Tadagaki, K.; Coge, F.; Gohier, A.; Delagrange, P.; Chavatte, P.; Jockers, R. Importance of the second extracellular loop for melatonin MT1 receptor function and absence of melatonin binding in GPR50. *Br. J. Pharmacol.* 2018, 175 (16), 3281−3297.

(34) Ahuja, S.; Hornak, V.; Yan, E. C.; Syrett, N.; Goncalves, J. A.; Hirshfeld, A.; Ziliox, M.; Sakmar, T. P.; Sheves, M.; Reeves, P. J.; Smith, S. O.; Eilers, M. Helix movement is coupled to displacement of the second extracellular loop in rhodopsin activation. *Nat. Struct. Mol. Biol.* 2009, 16 (2), 168−175.

(35) Venkatakrishnan, A. J.; Deupi, X.; Lebon, G.; Tate, C. G.; Schertler, G. F.; Babu, M. M. Molecular signatures of G-protein-coupled receptors. *Nature* 2013, 494 (7436), 185−194.

(36) Kang, Y.; Zhou, X. E.; Gao, X.; He, Y.; Liu, W.; Ishchenko, A.; Barty, A.; White, T. A.; Yefanov, O.; Han, G. W.; Xu, Q.; de Waal, P. W.; Ke, J.; Tan, M. H.; Zhang, C.; Moeller, A.; West, G. M.; Pascal, B. D.; Van Eps, N.; Caro, L. N.; Vishnivetskiy, S. A.; Lee, R. J.; Suino-Powell, K. M.; Gu, X.; Pal, K.; Ma, J.; Zhi, X.; Boutet, S.; Williams, G. J.; Messerschmidt, M.; Gati, C.; Zatsepin, N. A.; Wang, D.; James, D.; Basu, S.; Roy-Chowdhury, S.; Conrad, C. E.; Coe, J.; Liu, H.; Lisova, S.; Kupitz, C.; Grotjohann, I.; Fromme, R.; Jiang, Y.; Tan, M.; Yang, H.; Li, J.; Wang, M.; Zheng, Z.; Li, D.; Howe, N.; Zhao, Y.; Standfuss, J.; Diederichs, K.; Dong, Y.; Potter, C. S.; Carragher, B.; Caffrey, M.; Jiang, H.; Chapman, H. N.; Spence, J. C.; Fromme, P.; Weierstall, U.; Ernst, O. P.; Katritch, V.; Gurevich, V. V.; Griffin, P. R.; Hubbell, W. L.; Stevens, R. C.; Cherezov, V.; Melcher, K.; Xu, H. E. Crystal structure of rhodopsin bound to arrestin by femtosecond X-ray laser. *Nature* 2015, 523 (7562), 561−567.

(37) Dror, R. O.; Arlow, D. H.; Borhani, D. W.; Jensen, M. O.; Piana, S.; Shaw, D. E. Identification of two distinct inactive

conformations of the beta2-adrenergic receptor reconciles structural and biochemical observations. *Proc. Natl. Acad. Sci. U. S. A.* 2009, 106 (12), 4689−4694.

(38) Rasmussen, S. G.; Choi, H. J.; Fung, J. J.; Pardon, E.; Casarosa, P.; Chae, P. S.; Devree, B. T.; Rosenbaum, D. M.; Thian, F. S.; Kobilka, T. S.; Schnapp, A.; Konetzki, I.; Sunahara, R. K.; Gellman, S. H.; Pautsch, A.; Steyaert, J.; Weis, W. I.; Kobilka, B. K. Structure of a nanobody-stabilized active state of the beta(2) adrenoceptor. *Nature* 2011, 469 (7329), 175−180.

(39) Deupi, X.; Dolker, N.; Lopez-Rodriguez, M. L.; Campillo, M.; Ballesteros, J. A.; Pardo, L. Structural models of class a G protein-coupled receptors as a tool for drug design: insights on trans-membrane bundle plasticity. *Curr. Top. Med. Chem.* 2007, 7 (10), 991−998.

(40) Morgan, P. J.; Davidson, G.; Lawson, W.; Barrett, P. Both pertussis toxin-sensitive and insensitive g-proteins link melatonin receptor to inhibition of adenylate cyclase in the ovine pars tuberalis. *J. Neuroendocrinol.* 1990, 2 (6), 773−776.

(41) Giannone, F.; Malpeli, G.; Lisi, V.; Grasso, S.; Shukla, P.; Ramarli, D.; Sartoris, S.; Monsurro, V.; Krampera, M.; Amato, E.; Tridente, G.; Colombatti, M.; Parenti, M.; Innamorati, G. The puzzling uniqueness of the heterotrimeric G15 protein and its potential beyond hematopoiesis. *J. Mol. Endocrinol.* 2010, 44 (5), 259−269.

(42) Mende, F.; Hundahl, C.; Plouffe, B.; Skov, L. J.; Sivertsen, B.; Madsen, A. N.; Luckmann, M.; Diep, T. A.; Offermanns, S.; Frimurer, T. M.; Bouvier, M.; Holst, B. Translating biased signaling in the ghrelin receptor system into differential in vivo functions. *Proc. Natl. Acad. Sci. U. S. A.* 2018, 115 (43), E10255−E10264.

(43) Zimmerman, B.; Beautrait, A.; Aguila, B.; Charles, R.; Escher, E.; Claing, A.; Bouvier, M.; Laporte, S. A. Differential beta-arrestin-dependent conformational signaling and cellular responses revealed by angiotensin analogs. *Sci. Signaling* 2012, 5 (221), No. ra33.

(44) Garcia-Perganeda, A.; Pozo, D.; Guerrero, J. M.; Calvo, J. R. Signal transduction for melatonin in human lymphocytes: involvement of a pertussis toxin-sensitive G protein. *J. Immunol* 1997, 159 (8), 3774−3781.

(45) Jarzynka, M. J.; Passey, D. K.; Ignatius, P. F.; Melan, M. A.; Radio, N. M.; Jockers, R.; Rasenick, M. M.; Brydon, L.; Witt-Enderby, P. A. Modulation of melatonin receptors and G-protein function by microtubules. *J. Pineal Res.* 2006, 41 (4), 324−336.

(46) Karamitri, A.; Jockers, R. Melatonin in type 2 diabetes mellitus and obesity. *Nat. Rev. Endocrinol.* 2019, 15 (2), 105−125.

(47) Imam, A.; Winnebeck, E. C.; Buchholz, N.; Froguel, P.; Bonnefond, A.; Solimena, M.; Ivanova, A.; Bouvier, M.; Plouffe, B.; Charpentier, G.; Karamitri, A.; Jockers, R.; Roenneberg, T.; Vetter, C. Circadian, Sleep and Caloric Intake Phenotyping in Type 2 Diabetes Patients With Rare Melatonin Receptor 2 Mutations and Controls: A Pilot Study. *Front. Physiol.* 2020, 11, 564140.

(48) Owino, S.; Buonfiglio, D. D. C.; Tchio, C.; Tosini, G. Melatonin Signaling a Key Regulator of Glucose Homeostasis and Energy Metabolism. *Front. Endocrinol. (Lausanne, Switz.)* 2019, 10, 488.

(49) Buonfiglio, D.; Tchio, C.; Furigo, I.; Donato, J., Jr.; Baba, K.; Cipolla-Neto, J.; Tosini, G. Removing melatonin receptor type 1 signaling leads to selective leptin resistance in the arcuate nucleus. *J. Pineal Res.* 2019, 67 (2), No. e12580.

(50) Owino, S.; Sanchez-Bretano, A.; Tchio, C.; Cecon, E.; Karamitri, A.; Dam, J.; Jockers, R.; Piccione, G.; Noh, H. L.; Kim, T.; Kim, J. K.; Baba, K.; Tosini, G. Nocturnal activation of melatonin receptor type 1 signaling modulates diurnal insulin sensitivity via regulation of PI3K activity. *J. Pineal Res.* 2018, 64 (3), e12462.

(51) Contreras-Alcantara, S.; Baba, K.; Tosini, G. Removal of melatonin receptor type 1 induces insulin resistance in the mouse. *Obesity* 2010, 18 (9), 1861−1863.

(52) Balkau, B. [An epidemiologic survey from a network of French Health Examination Centres, (D.E.S.I.R.): epidemiologic data on the insulin resistance syndrome]. *Rev. Epidemiol Sante Publique* 1996, 44 (4), 373−375.

(53) Sladek, R.; Rocheleau, G.; Rung, J.; Dina, C.; Shen, L.; Serre, D.; Boutin, P.; Vincent, D.; Belisle, A.; Hadjadj, S.; Balkau, B.; Heude, B.; Charpentier, G.; Hudson, T. J.; Montpetit, A.; Pshezhetsky, A. V.; Prentki, M.; Posner, B. I.; Balding, D. J.; Meyre, D.; Polychronakos, C.; Froguel, P. A genome-wide association study identifies novel risk loci for type 2 diabetes. *Nature* **2007**, *445* (7130), 881−885.

(54) Meyre, D.; Delplanque, J.; Chevre, J. C.; Lecoeur, C.; Lobbens, S.; Gallina, S.; Durand, E.; Vatin, V.; Degraeve, F.; Proenca, C.; Gaget, S.; Korner, A.; Kovacs, P.; Kiess, W.; Tichet, J.; Marre, M.; Hartikainen, A. L.; Horber, F.; Potoczna, N.; Hercberg, S.; Levy-Marchal, C.; Pattou, F.; Heude, B.; Tauber, M.; McCarthy, M. I.; Blakemore, A. I.; Montpetit, A.; Polychronakos, C.; Weill, J.; Coin, L. J.; Asher, J.; Elliott, P.; Jarvelin, M. R.; Visvikis-Siest, S.; Balkau, B.; Sladek, R.; Balding, D.; Walley, A.; Dina, C.; Froguel, P. Genome-wide association study for early-onset and morbid adult obesity identifies three new risk loci in European populations. *Nat. Genet.* **2009**, *41* (2), 157−159.

(55) Leger, J.; Levy-Marchal, C.; Bloch, J.; Pinet, A.; Chevenne, D.; Porquet, D.; Collin, D.; Czernichow, P. Reduced final height and indications for insulin resistance in 20 year olds born small for gestational age: regional cohort study. *BMJ.* **1997**, *315* (7104), 341−347.

(56) Romon, M.; Lafay, L.; Bresson, J. L.; Oppert, J. M.; Borys, J. M.; Kettaneh, A.; Charles, M. A. Relationships between physical activity and plasma leptin levels in healthy children: the Fleurbaix-Laventie Ville Sante II Study. *Int. J. Obes.* **2004**, *28* (10), 1227−1232.

(57) Baron, M.; Maillet, J.; Huyvaert, M.; Dechaume, A.; Boutry, R.; Loiselle, H.; Durand, E.; Toussaint, B.; Vaillant, E.; Philippe, J.; Thomas, J.; Ghulam, A.; Franc, S.; Charpentier, G.; Borys, J. M.; Levy-Marchal, C.; Tauber, M.; Scharfmann, R.; Weill, J.; Aubert, C.; Kerr-Conte, J.; Pattou, F.; Roussel, R.; Balkau, B.; Marre, M.; Boissel, M.; Derhourhi, M.; Gaget, S.; Canouil, M.; Froguel, P.; Bonnefond, A. Loss-of-function mutations in MRAP2 are pathogenic in hyperphagic obesity with hyperglycemia and hypertension. *Nat. Med.* **2019**, *25* (11), 1733−1738.

(58) Lichtarge, O.; Bourne, H. R.; Cohen, F. E. An evolutionary trace method defines binding surfaces common to protein families. *J. Mol. Biol.* **1996**, *257* (2), 342−358.

(59) Katsonis, P.; Lichtarge, O. CAGI5: Objective performance assessments of predictions based on the Evolutionary Action equation. *Hum. Mutat.* **2019**, *40* (9), 1436−1454.

(60) Kenakin, T.; Christopoulos, A. Signalling bias in new drug discovery: detection, quantification and therapeutic impact. *Nat. Rev. Drug Discovery* **2013**, *12* (3), 205−216.

(61) Kenakin, T.; Watson, C.; Muniz-Medina, V.; Christopoulos, A.; Novick, S. A simple method for quantifying functional selectivity and agonist bias. *ACS Chem. Neurosci.* **2012**, *3* (3), 193−203.

(62) Koehl, A.; Hu, H.; Maeda, S.; Zhang, Y.; Qu, Q.; Paggi, J. M.; Latorraca, N. R.; Hilger, D.; Dawson, R.; Matile, H.; Schertler, G. F. X.; Granier, S.; Weis, W. I.; Dror, R. O.; Manglik, A.; Skiniotis, G.; Kobilka, B. K. Structure of the micro-opioid receptor-Gi protein complex. *Nature* **2018**, *558* (7711), 547−552.

(63) Lebon, G.; Warne, T.; Edwards, P. C.; Bennett, K.; Langmead, C. J.; Leslie, A. G.; Tate, C. G. Agonist-bound adenosine A2A receptor structures reveal common features of GPCR activation. *Nature* **2011**, *474* (7352), 521−525.

(64) Fredriksson, R.; Lagerstrom, M. C.; Lundin, L. G.; Schioth, H. B. The G-protein-coupled receptors in the human genome form five main families. Phylogenetic analysis, paralogon groups, and fingerprints. *Mol. Pharmacol.* **2003**, *63* (6), 1256−72.

(65) Isberg, V.; de Graaf, C.; Bortolato, A.; Cherezov, V.; Katritch, V.; Marshall, F. H.; Mordalski, S.; Pin, J. P.; Stevens, R. C.; Vriend, G.; Gloriam, D. E. Generic GPCR residue numbers - aligning topology maps while minding the gaps. *Trends Pharmacol. Sci.* **2015**, *36* (1), 22−31.

(66) Pettersen, E. F.; Goddard, T. D.; Huang, C. C.; Couch, G. S.; Greenblatt, D. M.; Meng, E. C.; Ferrin, T. E. UCSF Chimera−a visualization system for exploratory research and analysis. *J. Comput. Chem.* **2004**, *25* (13), 1605−1612.

(67) Webb, B.; Sali, A. Comparative Protein Structure Modeling Using MODELLER. *Curr. Protoc Protein Sci.* **2016**, *86*, 1−37.

(68) Zhou, X. E.; He, Y.; de Waal, P. W.; Gao, X.; Kang, Y.; Van Eps, N.; Yin, Y.; Pal, K.; Goswami, D.; White, T. A.; Barty, A.; Latorraca, N. R.; Chapman, H. N.; Hubbell, W. L.; Dror, R. O.; Stevens, R. C.; Cherezov, V.; Gurevich, V. V.; Griffin, P. R.; Ernst, O. P.; Melcher, K.; Xu, H. E. Identification of Phosphorylation Codes for Arrestin Recruitment by G Protein-Coupled Receptors. *Cell* **2017**, *170* (3), 457−469.